

Creep and fluidization in thermal amorphous solids

Samy Merabia, François Detcheverry
*Univ Lyon, Université Claude Bernard Lyon 1, CNRS,
 Institut Lumière Matière, F-69622, VILLEURBANNE, France*

When submitted to a constant mechanical load, many amorphous solids display power law creep followed by fluidization. A fundamental understanding of these processes is still far from being achieved. Here, we characterize creep and fluidization on the basis of a mesoscopic viscoplastic model that includes thermally activated yielding events and a broad distribution of energy barriers, which may be lowered under the effect of a local deformation. We relate the creep exponent observed before fluidization to the width of barrier distribution and to the specific form of stress redistribution following yielding events. We show that Andrade creep is accompanied by local strain-hardening driven by stress redistribution and find that the fluidization depends exponentially on the applied stress. The simulation results are interpreted in the light of a mean-field analysis, and should help in rationalizing the creep phenomenology of amorphous solids.

I. INTRODUCTION

Creep is observed in a wide variety of materials including crystalline metals¹, soft crystals², polymeric and metallic glasses^{3,4}, colloidal glasses^{5,6} and gels^{7,8}, and everyday complex fluids⁹. Typically, the strain first increases with time following a power law regime often described as Andrade creep, with $\epsilon(t) \sim t^p$ and a creep exponent p between 0 and 1. This creep regime is eventually interrupted by fluidization, after an elapsed time that decreases with the applied stress. Though the creep phenomenology is widespread, to date its understanding remains only partial^{10,11}, in particular for the underlying physical mechanism at play. Creep in metals is traditionally interpreted in terms of depinning and collective motion of dislocations^{1,12}. No such framework exists for amorphous solids.

While molecular simulations may provide a wealth of information on mechanical properties of disordered solids¹³, the slow kinetics inherent to creep make it prohibitive to reach fluidization time. Following the pioneering work of Bulatov and Argon¹⁴, mesoscopic models appear as an alternative to bridge both time and length scales between the molecular level and macroscopic, finite elements calculations¹³. The common idea is to coarse-grain fast microscopic motions, and retain only a minimal description of local plastic rearrangements or shear transformation zones (STZs), most importantly the long-range consequences of a single localized plastic event. Therefore, the essential ingredients include a local yielding probability, and a spatially resolved dynamics for the stress redistribution, often described by an Eshelby form. While elasto-plastic models have now generated a sustained line of research^{11,15–17}, with much scrutiny on the the shear steady state, comparatively little attention has been devoted to analyze the creep dynamics in amorphous solids. Two noticeable exceptions are a spatially resolved Soft Glassy Rheology model¹⁸ and a recent study by Boute and Vandembroucq¹⁹, which, however, is restricted to logarithmic creep only.

The purpose of this letter is to propose an interpre-

tation of creep on the basis of a mesoscopic model. We focus on thermal amorphous solids, such as polymeric or metallic glasses, for which flow proceeds through thermally activated localized events, and are characterized by a wide distribution of activation barriers. Using a combination of numerical simulations and a mean-field analysis, we investigate how the creep exponent relates to the barrier distribution and show the role of the stress redistribution in the creep dynamics. Interestingly, the mesoscopic model reveals local strain-hardening during the creep regime: some regions may accumulate large levels of local stress, while others see their local stress decrease with the global shear rate. Such strain-hardening phenomenon, which differs from that seen in metals, eventually triggers the fluidization of the material and allows to propose a simple law for the fluidization time.

II. MODEL

Our mesoscopic description relies on three main ingredients: a distribution of yielding barriers, possibly modified by mechanical effect, thermal activation, and stress redistribution. The system is divided into a collection of representative elements whose dimension corresponds to the size of a plastic event, and whose state is specified by an intrinsic energy barrier E and a local mechanical stress σ , assumed to be a scalar for simplicity. In a way similar to Eyring's model, thermal activation can trigger yielding with a rate

$$\lambda(E, \sigma) = \tau_m^{-1} \exp \left[-\frac{E - h(\sigma)}{k_B T} \right]. \quad (1)$$

Here, τ_m is a microscopic time, k_B is the Boltzmann constant and T is the temperature. The function $h(\sigma)$ specifies how the barrier may be lowered by the local stress; we will mainly consider a quadratic mechanical activation term $h(\sigma) = \sigma^2 v_a / (4\mu k_B T)$, where v_a is an activation volume, μ the infinite frequency shear modulus²⁰. After yielding, an element has his intrinsic barrier renewed from a distribution $\rho_E(E)$, its local stress put

to zero, and the stress it carried is redistributed to other elements.

Three types of stress redistribution are possible: “Eshelby”, “mean-field” and “short-range”. The former originates in the Eshelby problem of an inclusion in an elastic matrix and its propagator is quadrupolar^{15,21}

$$G_{ij} = \frac{2}{\pi r_{ij}^2} \cos(4\theta_{ij}) \quad (2)$$

where G_{ij} is the contribution received by site i from a site j , $r_{ij} = |\mathbf{r}_{ij}|$ is the distance between the two sites, and $\cos\theta_{ij} = (\mathbf{r}_{ij} \cdot \mathbf{e}_x)/r_{ij}$, where \mathbf{e}_x is a unit vector along the direction of shear. The mean-field propagator completely neglects spatial dependence and assign to all elements an identical contribution $G_{ij} = 1/(N-1)$, N being the total number of sites. To further assess the influence of the redistribution type, we will also consider a short-range propagator²², for which the stress carried by an element is redistributed only to its nearest neighbours, as described in Ref.²³.

To fully specify the model, it remains to choose the probability density of intrinsic barrier energy $\rho_E(E)$. In the following, we will concentrate mostly on a Gaussian distribution with mean \bar{E} and variance Δ^2 ,

$$\rho_E(E) = \frac{1}{\sqrt{2\pi\Delta^2}} \exp\left[-\frac{(E-\bar{E})^2}{2\Delta^2}\right]. \quad (3)$$

Such a Gaussian form is often assumed in modelling the plastic behaviour of polymer glasses²⁴, or more generally molecular glasses^{25,26}. Furthermore, it has been long recognized to be associated with a stretched exponential relaxation functions^{26,27}. For the sake of analytical tractability, we will also consider a barrier distribution which is exponential and has a width α^{-1} ,

$$\rho_E(E) = \alpha \exp[-\alpha(E - E_o)] H[E - E_o], \quad (4)$$

where E_o denotes the minimal energy barrier and H is the Heaviside distribution, $H(x) = 1$ if $x > 0$ and $H(x) = 0$ otherwise. The model is close to that of Ref.¹⁹, but the distribution of energy barriers has a width which is finite rather than infinite, hence logarithmic creep is never observed.

III. SIMULATIONS

To solve the model numerically, we discretize space with a two-dimensional square lattice and periodic boundary conditions. Initially, each site i carries the same stress σ_0 , and is assigned an energy barrier E_i sampled from the steady distribution $\rho_E(E_i) \exp(E_i/k_B T)$. The creep process is simulated using a Kinetic Monte Carlo (KMC) algorithm²⁸. Given the yielding rates specified by Eq. (1) for all sites, each iteration selects a site i to yield, and generates a corresponding time increment. Upon yielding, the local stresses and the total strain are updated as follows,

$$\sigma_i \rightarrow 0, \quad \sigma_j \rightarrow \sigma_j + G_{ij}\sigma_i^- \text{ for } j \neq i, \quad \epsilon \rightarrow \epsilon + \sigma_i^-/2\hbar$$

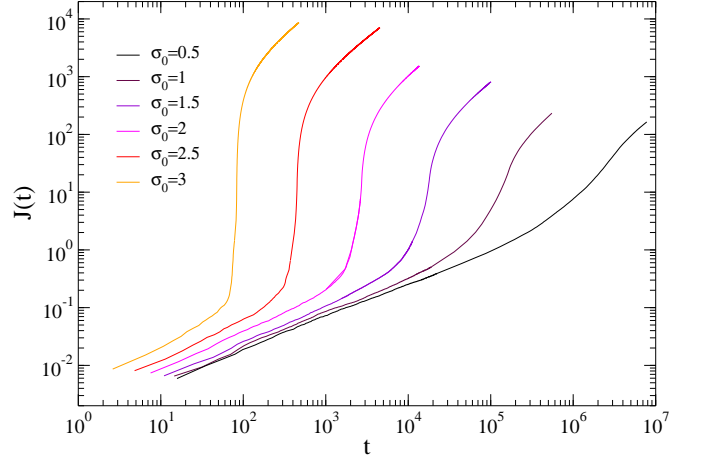


FIG. 1. Creep compliance in simulations. The stress redistribution is of Eshelby type, and the distribution of energy barrier is Gaussian with $\Delta = 3$. Different values of applied stress σ_0 are shown.

where σ_i^- is the stress carried by the site i prior to yielding. A new barrier energy is then chosen from the probability density ρ_E . We use a pseudo-spectral method to carry out the elastic redistribution¹⁵, and impose the sum rule $\forall i, \sum_{j \neq i} G_{ij} = 1$, so that the spatially averaged stress $\frac{1}{N} \sum_i \sigma_i = \sigma_0$ remains constant at all time, as required by the creep set-up. We have simulated systems with typical linear size 64 and 256, and verified that the results are not size dependent. In data presented below, we take $k_B T$ as energy unit, express stress in units where the shear modulus is $\mu = 1$, and choose the time unit as $\tau_m \exp(\bar{E})$ or $\tau_m \exp(E_o)$ in the Gaussian and exponential case respectively. Finally, the activation parameter is set to $v_a = 1$. Once this choice is made, the only remaining parameter of the model is the distribution width Δ or α^{-1} . If not indicated otherwise, the stress redistribution is of Eshelby form, and ρ_E is Gaussian.

Figure 1 summarizes the creep phenomenology of our model. Whatever the applied stresses σ_0 , three regimes may be distinguished in the compliance curve $J(t) = \epsilon(t)/\sigma_0$. At early times, the compliance increases algebraically with time $J(t) \sim t^p$, where the creep exponent p is found to be almost independent of σ_0 . This first regime terminates with a sharp increase in deformation, at a fluidization time t_f that decreases with the applied stress σ_0 . The system eventually settles into steady flow, where the strain increases linearly with time, $J(t) \sim t$. Below we investigate in turn the primary creep and fluidization. To do so, we now develop a mean-field theory.

IV. MEAN-FIELD ANALYSIS

When spatial dependence is entirely discarded, the system is completely described by the probability density $P(E, \sigma, t)$ to find at time t an element with energy bar-

rier E and subject to a stress σ . Our starting point is the evolution equation

$$\partial_t P = -\lambda(E, \sigma)P + Y(t)\rho_E(E)\delta(\sigma) - S(t)\partial_\sigma P, \quad (6)$$

where $Y(t) = \langle \lambda(E, \sigma) \rangle_P$, $S(t) = \langle \sigma \lambda(E, \sigma) \rangle_P$ and $\langle \cdot \rangle_P$ denotes an average over the full distribution $P(E, \sigma, t)$. In the RHS of Eq. (6), the first term originates from elements in state (E, σ) that yield with a rate $\lambda(E, \sigma)$. $Y(t)$ is the average yielding rate, also called material's fluidity¹⁸. Elements that have yielded arrive in a renewed state with zero stress and an energy barrier randomly chosen in the distribution $\rho_E(E)$. The average rate of released stress $S(t)$ gathers the contributions from all yielding elements, which is redistributed equally throughout the system, resulting in a drift term in σ with velocity $S(t)$. One can check that the evolution equation implies two conserved quantities: the total probability and the total stress. While Eq. (6) may be written directly, a derivation is possible starting from a Boltzmann equation involving a stress collision operator.

The model defined here is related but distinct from the Soft Glassy Rheology (SGR) model²⁹. With quadratic activation function $h(\sigma) \sim \sigma^2$ and an exponential $\rho_E(E)$, the model is formally equivalent to SGR with noise temperature $x = \alpha$. However, the interpretation is completely different, since as in the original trap model²⁷, T here is really the temperature, not an effective noise resulting from yielding events elsewhere in the material. It was pointed out that the mechanical noise in SGR should be “determined self-consistently by the interactions in the system”³⁰. This key point is captured by the redistribution term $S(t)\partial_\sigma$, and is crucial for the creep situation, a transient regime. In contrast to steady shear where the noise temperature is constant, the activity here is time-dependent, as it slowly declines during creep. Our description is also reminiscent of fiber bundles model (FBM) but differs in an essential way^{31,32}. In contrast to fibers that permanently disappear once ruptured, elements that have yielded are renewed and will again carry a stress. The mean-field analysis is used in the following to provide a qualitative understanding ; to a large extent, it proves sufficient to rationalize what occurs in more realistic cases.

V. CREEP REGIME

We first consider the mean-field model and seek the total strain $\epsilon(t) = \int_0^t S(t)/2\mu$ that follows a stress step. The model can be solved if we neglect non-linear effects by setting $h(\sigma) = 0$. In that case, the yielding of an element depends only on the time elapsed since its latest renewal and $Y(t)$ can be computed without any reference to the local stress. The distribution of barriers is in a steady state characterized by

$$P_{\text{st}}(\tau) = \frac{\tau\rho(\tau)}{\langle \tau \rangle}, \quad Y_{\text{st}} = \frac{1}{\langle \tau \rangle}, \quad (7)$$

where, from now on, we use the intrinsic yielding time $\tau = e^E$ rather than the energy barrier, and $\langle \cdot \rangle$ denotes an average over the corresponding distribution $\rho(\tau)$. The initial condition involves a uniform load on all elements and an equilibrated distribution of barriers, namely $P(\tau, \sigma, t = 0) = P_{\text{st}}(\tau)\delta(\sigma - \sigma_0)$. We do not consider aging effects.

To solve the model, let's introduce $\bar{\sigma}(\tau, t) = \int d\tau \sigma P(\tau, \sigma, t)$ which satisfies

$$\partial_t \bar{\sigma} = -\frac{\bar{\sigma}}{\tau} + S(t)P_{\text{st}}(\tau), \quad S(t) = \int \frac{d\tau}{\tau} \bar{\sigma}(\tau, t). \quad (8)$$

Using the condition $\int dt \bar{\sigma}(\tau, t) = \sigma_0$ that holds at all time, and working with Laplace transforms, one obtains the exact solution, valid for any distribution of barriers,

$$\frac{S(s)}{\sigma_0} = \frac{1}{sR(s)} - 1, \quad R(s) = \int d\tau \frac{P_{\text{st}}(\tau)}{s + \tau^{-1}}, \quad (9)$$

where s is the Laplace variable and indicates the nature of the function. Note that Eq. (9) can be rewritten as $J(s)G(s) = 1/s^2$, where $J(s) = \epsilon(s)/\sigma_0$ is the compliance, and $G(s) = \mu R(s)$ is the relaxation modulus³³. The explicit expression $G(t) = \mu \int_0^\infty P_{\text{st}}(\tau) e^{-t/\tau} d\tau$ has a simple interpretation. The integral is the average fraction of elements that have never yielded at time t , suggesting that sites that have already yielded at least once do not play any role, as if disappearing in FBM-like models. This interpretation is surprising at first sight but understandable with the analysis of local stress presented below.

Though $R(s)$ can be obtained in closed form for some barrier distributions, taking the inverse Laplace transform of $1/R(s)$ proves impossible. Accordingly, we resort to a small- s expansion and relying on Tauberian theorems³⁴, we extract the asymptotic behavior of $S(t)$. For the sake of tractability, we consider an exponential distribution of barrier as defined in Eq. (4), which translates into a power law distribution of yielding time $\rho(\tau) = \alpha\tau_o^\alpha/\tau^{\alpha+1}H[\tau - \tau_o]$, with τ_o the minimum value. Assuming $\alpha > 1$, $R(s)$ can be expressed in terms of hypergeometric function as $sR(s) = {}_2F_1(1, -1 + \alpha, \alpha, -1/\tau_o s)$. Several cases arise for the asymptotic behavior. If $\alpha > 2$, then the long-time behavior is Newtonian with $S(t) \sim \langle \tau \rangle / \langle \tau^2 \rangle$, a result that holds more generally for any distribution $\rho(\tau)$ whose variance $\langle \tau^2 \rangle$ is finite. In the marginal case $\alpha = 2$, one gets $S(t) \sim 1/\ln(t/\tau_o)$. More importantly, when $1 < \alpha < 2$, $S(t) \sim t^{\alpha-2}$, implying that the creep exponent is $p = \alpha - 1$. Though the starting point given by Eq. (6) is different, those conclusions are in agreement with Ref.²⁹. We do not consider the case $\alpha < 1$, as we assume that the mean yielding $\langle \tau \rangle$ is finite so that an equilibrated state exists. In the limit $\alpha \rightarrow 1^+$, the behavior approaches logarithmic creep, since $\langle \tau \rangle$ grows without bound and there are no more time scale in the system.

While those conclusions have been reached for an exponential $\rho_E(E)$, corresponding to a power law $\rho(\tau)$,

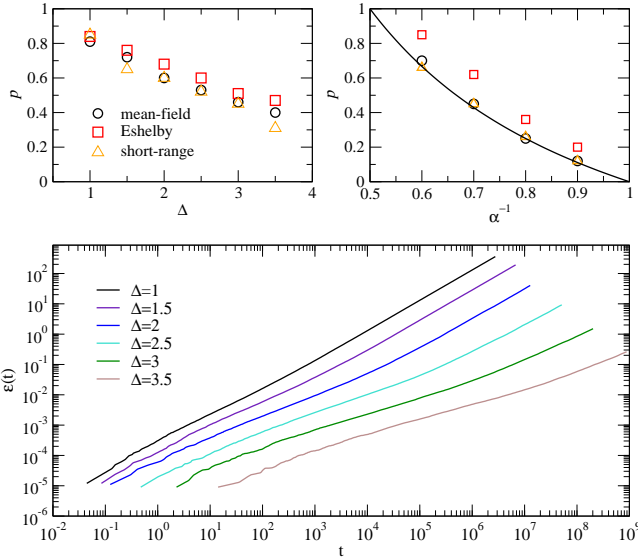


FIG. 2. Creep regime and exponent. (Bottom) Strain curves with Eshelby redistribution and Gaussian ρ_E of various width Δ . The applied stress is $\sigma_o = 0.01$. (Top) Creep exponent, as defined in the text, for three types of stress propagators, and for Gaussian and exponential ρ_E (left and right respectively). In the latter, the line is the mean-field prediction. Symbol size is indicative of error bars.

they are informative of other situations. First, if yielding times are bounded by a maximal value τ_{\max} , the long-time behavior is ultimately Newtonian but up to $t \simeq \tau_{\max}$, we expect a transient regime similar to the asymptotic behavior described above. Second, as soon as the distribution of energy is not narrowly peaked, there are widely different yielding times, and we expect that the creep exponent directly reflects the width of energy distribution.

With the mean-field prediction in hand, we now examine how the creep properties is affected by the type of stress redistribution and the choice of energy barrier. As a quantitative measure, we focus on the exponent characterizing the primary creep regime. In practice, a linear fit to $\epsilon(t)$ in bilogarithmic scale was used to get at all time an “effective exponent”, the minimum of which is the creep exponent reported in Fig. 2. If ρ_E is exponential, the asymptotic behavior is $\epsilon(t) \sim t^p$, and the minimum is attained in a plateau at the longest time. If ρ_E is Gaussian, or bounded, then $\epsilon(t) = ct^p + t/\eta$, with c a constant and η the viscosity⁷ ³⁵. The effective exponent exhibits a minimum near the crossover between the two regimes, which, to be seen, may require very long simulations, reaching up to 10^9 KMC iterations. As shown in Fig. 2 (top right), the simulation data for the exponential ρ_E is in full agreement with the mean-field prediction $p = \alpha - 1$. Should we expect a similar result with Eshelby and short-range redistributions? On the one hand, given the long-range nature of elastic propagator, the mean-field theory could be expected to be exact³⁶. On the other hand, it was argued that the stress resulting from spatially distributed

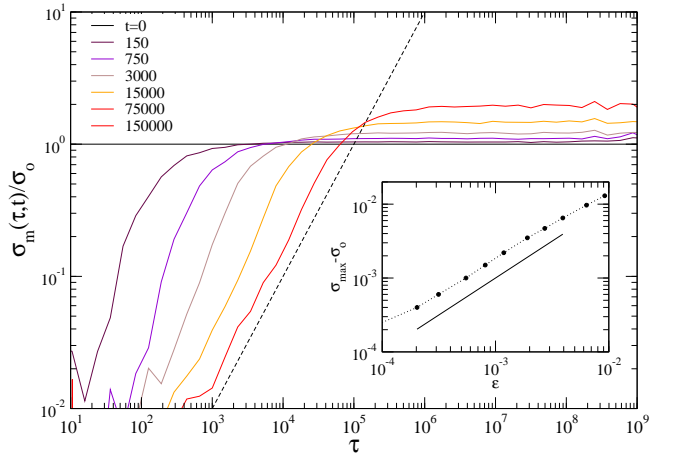


FIG. 3. Analysis of local stress during creep. The main graph shows how the mean stress $\sigma_m(\tau, t)$ carried by sites with yielding time τ evolves in time. A plateau is seen at large τ . (Inset) Plateau value, indicating the mean stress carried by “slow” elements, as a function of strain. The dashed and solid lines have slope unity. The simulation involves Eshelby redistribution, Gaussian ρ_E with $\Delta = 3$ and $\sigma_o = 0.01$.

events is “dominated by local contributions”^{15,37}. Surprisingly, we find that within numerical accuracy, the mean-field and short-range exponent coincide, whereas the Eshelby case yields consistently higher values. This observation also applies to the Gaussian case. Overall, we see that the wider the barrier distribution, the slower the creep, but the value of creep exponent is sensitive to both the specific distribution of barriers and the form of the stress propagator.

VI. LOCAL STRESS

To get further insight in the mesoscopic dynamics during the creep regime, we have conducted an analysis of the local stress carried by elements. Of particular attention is the relation between the local stress σ_i carried by an element i , and its instantaneous yielding time τ_i . Figure 3 reveals a strongly heterogeneous dynamics during primary creep. Indeed, “fast” elements having a low energy barrier carry on average a small amount of stress $\sigma_i \ll \sigma_o$, while “slow” elements support most of the stress. Noticeably, the level of stress borne by these elements increases with time. As shown in the inset of Fig. 3, this increase is approximately proportional to the local strain $\epsilon(t)$. Such strain-hardening, here understood as an increase in local stress required to produce additional strain, may be simply explained in the framework of the mean-field analysis presented above. Using Eqs. (8)-(9), one gets for $\sigma_m(\tau, t)$, the mean stress carried at time t by elements with yield time τ ,

$$\sigma_m(\tau, s) = \frac{\bar{\sigma}(\tau, s)}{P_{st}(\tau)} = \frac{\sigma_o + S(s)}{s + \tau^{-1}}. \quad (10)$$

and obtain in the two limits,

$$\tau \ll t, \quad \sigma_m(\tau, t) = \mu\tau\dot{\epsilon}(t), \quad (11a)$$

$$\tau \gg t, \quad \sigma_m(\tau, t) = \mu\epsilon(t) + \sigma_o. \quad (11b)$$

Schematically, one can identify two populations of sites, respectively fast and slow depending on the value of the local yielding time τ as compared to the elapsed time t . On the one hand, the sites that have yielded already and that are carrying a stress decreasing in time as $\dot{\epsilon}(t)$. On the other hand, the resistant sites that have not yielded yet, and who carry a stress increasing as $\epsilon(t)$. In Fig. 3, one sees that Eqs. (11a) and (11b) apply to a good approximation, even though the propagator is of Eshelby type rather than mean-field.

VII. FLUIDIZATION TIME

At the fluidization transition, the deformation increases sharply, and we have observed strain localization, as already noticed in Ref.¹⁸. In particular, the standard deviation of the local strain goes through a maximum, which is used to pinpoint the fluidization time t_f . Figure 4 reveals an exponential dependence of the fluidization time $t_f(\sigma_o)$ on the applied stress.

To rationalize this behavior, we make use of two observations. First, the strain at fluidization $\epsilon_f = \epsilon(t_f)$ varies only weakly with σ_o , namely $\epsilon_f(\sigma_o) \approx \dot{\epsilon}_f - \zeta\sigma_o$, as previously observed in some experiments^{2,9}. Second, the particular form of $h(\sigma)$ does not appear to have the leading role in the $t_f(\sigma_o)$ relation since we also found an exponential dependence when $h(\sigma)$ is linear rather than quadratic. Consider the plateau in σ associated to slow sites, which at a time t , ranges from t to τ_{\max} , the largest relaxation time in the system. We reintroduce the effect of activation in an approximate manner, with $\sigma(t)$ estimated from the solution with no activation term ($h = 0$) found above, thus leading to a shift factor $\exp[-h(\sigma_m(\tau, t))]$ for an element with intrinsic time τ . Now, we postulate that the fluidization occurs where there is no more element whose actual relaxation time is longer than the elapsed time,

$$t_f = \tau_{\max} \exp[-h(\sigma_o + \mu\epsilon_f)], \quad (12)$$

that is, activation effects have shifted the longest intrinsic relaxation time to a value below t_f . Assuming ϵ_f is strictly independent of σ_o , and expanding at first order in $\sigma_o \ll \mu\epsilon_f$, one gets

$$t_f = C \exp[-\sigma_o/\tilde{\sigma}], \quad (13)$$

with $C = \tau_{\max} \exp[-h(\mu\epsilon_f)]$ and $\tilde{\sigma} = 1/h'(\mu\epsilon_f)$. A similar argument applies if $\epsilon_f(\sigma_o)$ exhibits a linear dependence as considered above. As regards the dependence in the width Δ of barrier distribution, we note that the prefactor C may change significantly, as τ_{\max} increases with Δ . In experiments, alongside power law dependence for carbopol gels^{38,39}, an exponential $t_f(\sigma_o)$ was

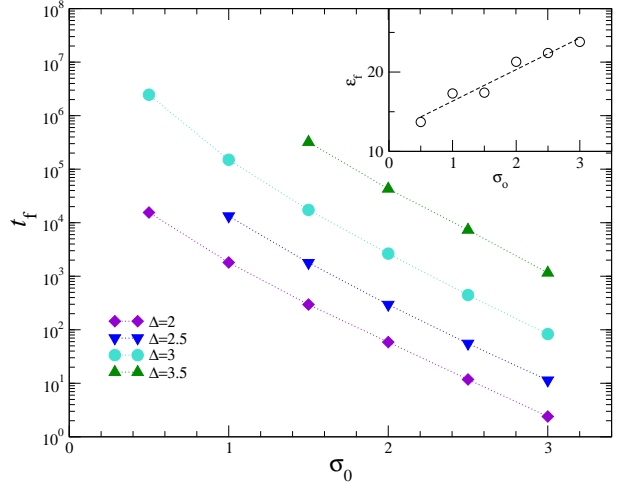


FIG. 4. Fluidization time t_f as a function of the applied stress σ_o . (Inset) Strain at fluidization ϵ_f as a function of σ_o . The dashed line is a linear fit. Here, redistribution is of Eshelby type, ρ_E is Gaussian with width Δ .

reported in carbon black gels^{7,8}, thermo-reversible silica gels⁴⁰ and protein gels⁴¹. Within our mesoscopic model, this phenomenology can be attributed to activated dynamics with energy barriers that are lowered by the applied stress.

Before concluding, we briefly comment on the steady state reached after fluidization, that is characterized by a constant shear rate $\dot{\gamma}$, as observed in colloidal glasses⁵. Simulations show that the final state attained during steady creep is identical to that reached upon constant deformation rate $\dot{\gamma}$. For exponential barrier distribution, the flow curve indicates a power law fluid $\sigma \sim \dot{\gamma}^\alpha$, in agreement with a mean-field analysis. In the Gaussian case, one finds a logarithmic behavior $\sigma \sim \ln(\dot{\gamma})$.

VIII. CONCLUSION

Through the consideration of a mesoscopic viscoplastic model, we demonstrated that the creep dynamics is directly related to distribution of energy barriers, and to the form of the stress redistribution subsequent to yielding. Moreover, our simulations show that primary creep regime is accompanied by local strain-hardening, resulting from the existence of a broad distribution of yielding times. Strain hardening is also key to understand the fluidization process, which here displays an exponential dependence on the applied stress, as seen in experiments on colloidal gels. We have focused on amorphous solids where thermally activated yielding events play the leading role. Creep and fluidization are also observed in athermal systems such as carbopol gels^{38,39}, which are yield stress fluids. It remains to address this important class of materials.

IX. ACKNOWLEDGEMENTS

We are grateful to C. Barentin, M. Le Merrer and L. Vanel, as well as T. Divoux and S. Manneville, for

introducing us to the phenomenology of creep in soft materials and for stimulating discussions. Part of the simulations have been run at PSMN, Pôle Scientifique de Modélisation Numérique, Lyon.

¹ M.-C. Miguel, A. Vespignani, M. Zaiser, and S. Zapperi, Phys. Rev. Lett. **89**, 165501 (2002).

² T. Bauer, J. Oberdisse, and L. Ramos, Phys. Rev. Lett. **97**, 258303 (2006).

³ T. Egami, T. Iwashita, and W. Dmowski, Metals **3**, 77 (2013).

⁴ R. A. Riggelman, K. S. Schweizer, and J. J. De Pablo, Macromolecules **41**, 4969 (2008).

⁵ M. Siebenbürger, M. Ballauff, and T. Voigtmann, Phys. Rev. Lett. **108**, 255701 (2012).

⁶ T. Sentjabrskaja, P. Chaudhuri, M. Hermes, W. C. K. Poon, J. Horbach, S. U. Egelhaaf, and M. Laurati, Sci. Rep. **5**, 11884 (2015).

⁷ T. Gibaud, D. Frelat, and S. Manneville, Soft Matter **6**, 3482 (2010).

⁸ V. Grenard, T. Divoux, N. Taberlet, and S. Manneville, Soft Matter **10**, 1555 (2014), arXiv:1310.0385.

⁹ F. Caton and C. Baravian, Rheol. Acta **47**, 601 (2008).

¹⁰ D. Bonn, J. Paredes, M. M. Denn, L. Berthier, T. Divoux, and S. Manneville, arXiv , 1502.05281 (2015), arXiv:1502.05281.

¹¹ T. Voigtmann, Curr. Opin. Colloid Interface Sci. **19**, 549 (2014).

¹² F. Louchet and P. Duval, Int. J. Mater. Res. **100**, 1433 (2009).

¹³ D. Rodney, A. Tanguy, and D. Vandembroucq, Modelling Simul. Mater. Sci. Eng. **19**, 083001 (2011).

¹⁴ V. V. Bulatov and a. S. Argon, Modelling Simul. Mater. Sci. Eng. **2**, 167 (1999).

¹⁵ G. Picard, A. Ajdari, F. Lequeux, and L. Bocquet, Eur. Phys. J. E. **15**, 371 (2004).

¹⁶ K. Martens, L. Bocquet, and J.-L. Barrat, Phys. Rev. Lett. **106**, 156001 (2011).

¹⁷ A. Nicolas, K. Martens, L. Bocquet, and J.-L. Barrat, Soft Matter **10**, 4648 (2014).

¹⁸ S. Fielding, Rep. Prog. Phys. **77**, 102601 (2014).

¹⁹ D. Bouttes and D. Vandembroucq, AIP Conference Proceedings , 481 (2013).

²⁰ E. R. Homer, D. Rodney, and C. A. Schuh, Phys. Rev. B **81**, 064204 (2010).

²¹ J. Eshelby, Proc. R. Soc. London, Ser. A **241**, 467 (1957).

²² G. S. Daehn, Acta Mater. **49**, 2017 (2001).

²³ K. Martens, L. Bocquet, and J.-L. Barrat, Soft Matter **8**, 4197 (2012).

²⁴ O. A. Hasan and M. C. Boyce, Polym. Eng. Sci. **35**, 331344 (1995).

²⁵ W. Shirmacher, G. Ruocco, and V. Mazzone, Phys. Rev. Lett. **115**, 015901 (2015).

²⁶ X. Xia and P. G. Wolynes, Phys. Rev. Lett. **86**, 5526 (2001).

²⁷ C. Monthus and J.-P. Bouchaud, J. Phys. A: Math. Gen. **29**, 3847 (1996).

²⁸ A. B. Bortz, M. H. Kalos, and J. L. Lebowitz, J. Comput. Phys. **17**, 10 (1975).

²⁹ S. M. Fielding, P. Sollich, and M. E. Cates, J. Rheol **44**, 323 (2000).

³⁰ P. Sollich, Phys. Rev. E **58**, 738 (1998), arXiv:9712001 [cond-mat].

³¹ R. Hidalgo, F. Kun, and H. Herrmann, Phys. Rev. E **65**, 032502 (2002).

³² S. Pradhan, A. Hansen, and B. K. Chakrabarti, Rev. Mod. Phys. **82**, 499 (2010).

³³ W. Findley, J. Lai, and K. Onaran, *Creep and relaxation of nonlinear viscoelastic materials* (Dover, 1978).

³⁴ W. Feller, *An introduction to probability theory and its applications, Volume II*, 2nd ed. (John Wiley & Sons, 1971).

³⁵ Y. Gueguen, V. Keryvin, T. Rouxel, M. Le-Fur, H. Orain, B. Bureau, C. Boussard-Plédel, and J.-C. Sangleboeuf, Mechanics of Materials **85**, 47 (2015).

³⁶ K. Dahmen, Y. Ben-Zion, and J. Uhl, Phys. Rev. Lett. **102**, 175501 (2009).

³⁷ S. M. Fielding, M. E. Cates, and P. Sollich, Soft Matter **5**, 2378 (2009).

³⁸ T. Divoux, D. Tamarii, C. Barentin, and S. Manneville, Phys. Rev. Lett. **104**, 208301 (2010).

³⁹ T. Divoux, D. Tamarii, C. Barentin, S. Teitel, and S. Manneville, Soft Matter **8**, 4151 (2012).

⁴⁰ V. Gopalakrishnan and C. F. Zukoski, J. Rheol. **51**, 623 (2007).

⁴¹ S. B. Lindström, T. E. Kodger, J. Sprakler, and D. A. Weitz, Soft Matter **8**, 3657 (2012).